J|A|C|S
ARTICLES
Published on Web 01/16/2004

Electron Transfer at Self-Assembled Monolayers Measured by Scanning Electrochemical Microscopy

Biao Liu,[†] Allen J. Bard,*[,†] Michael V. Mirkin,*[,‡] and Stephen E. Creager[§]

Contribution from the Department of Chemistry and Biochemistry, The University of Texas at Austin, Austin, Texas 78712, Department of Chemistry and Biochemistry, Queens College−CUNY, Flushing, New York 11367, and Department of Chemistry, Clemson University, Clemson, South Carolina 29634-1905

Received September 19, 2003; E-mail: ajbard@mail.utexas.edu

Abstract: New approaches have been developed for measuring the rates of electron transfer (ET) across self-assembled molecular monolayers by scanning electrochemical microscopy (SECM). The developed models can be used to independently measure the rates of ET mediated by monolayer-attached redox moieties and direct ET through the film as well as the rate of a bimolecular ET reaction between the attached and dissolved redox species. By using a high concentration of redox mediator in solution, very fast heterogeneous (10^8 s^{-1}) and bimolecular (10^{11} mol^{-1} cm^3 s^{-1}) ET rate constants can be measured. The ET rate constants measured for ferrocene/alkanethiol on gold were in agreement with previously published data. The rates of bimolecular heterogeneous electron transfer between the monolayer-bound ferrocene and water-soluble redox species were measured. SECM was also used to measure the rate of ET through nonelectroactive alkanethiol molecules between substrate gold electrodes and a redox probe ($Ru(NH_3)_6^{3+}$) freely diffusing in the solution, yielding a tunneling decay constant, β, of 1.0 per methylene group.

Introduction

The elucidation of long-range bridge-mediated electron transfer (ET) is an important problem in modern chemistry and biology.[1,2] In addition to the fundamental interest, understanding and controlling charge transport through molecular films of nanometer thickness are relevant to technological systems such as molecular electronics and sensor design.[3,4] Self-assembled monolayers (SAMs) of alkanethiols have been widely used as the bridging moieties. The well-ordered, close-packed nature of the monolayer and the almost unlimited possibility of introducing functional groups in alkanethiols make SAMs of alkanethiols suitable models for investigating ET across molecular films.[5] The kinetics of ET across SAMs with functional redox groups or reactants dissolved in solution has been studied by a variety of experimental approaches including photochemical, electrochemical, and temperature jump techniques.[1,5−18] The ET rate constant, k_{et}, was measured as a function of the distance, r, between the electrode and a redox species. In general, for nonresonant tunneling, the rate constant decreases exponentially with increasing r, with values of the decay constant β ($= -d \ln[k_{et}]/dr$) ranging from 0.8 to 1.5 $Å^{-1}$ for saturated bridges and 0.2 to 0.6 $Å^{-1}$ for unsaturated bridges.[4,19,20]

Transient electrochemical techniques, like cyclic voltammetry and chronoamperometry, have been most commonly used for measuring the rates of ET through alkanethiol monolayers.[5,6,9] In cyclic voltammetry, the rate constants were typically obtained from the difference of the peak potentials, as suggested by Laviron.[21] In chronoamperometry, a potential step is applied to the working electrode and the ET rate constant can be determined from the current transient. Both techniques are experimentally straightforward and allow one to observe changes in rate constant over a wide range of potentials. However, these methods are burdened by the effects the resistive potential drop and double layer charging current, which affect the reliability

[†] The University of Texas at Austin.
[‡] Queens College−CUNY.
[§] Clemson University.

(1) (a) Barbara, P. F.; Meyer, T. J.; Ratner, M. A. *J. Phys. Chem.* **1996**, *100*, 13148. (b) Adams, D. M.; Brus, L.; Chidsey, C. E. D.; Creager, S.; Creutz, C.; Kagan, C. R.; Kamat, P. V.; Lieberman, M.; Lindsay, S.; Marcus, R. A.; Metzger, R. M.; Michel-Beyerle, M. E.; Miller, J. R.; Newton, M. D.; Rolison, D. R.; Sankey, O.; Schanze, K. S.; Yardley, J.; Zhu, X. *J. Phys. Chem. B* **2003**, *107*, 6668−6697.
(2) *Structure and Bonding: Long-Range Electron Transfer in Biology*; Springer-Verlag: New York, 1991.
(3) Willner, I.; Katz, E. *Angew. Chem., Int. Ed.* **2000**, *39*, 1181.
(4) Fox, M. A. *Acc. Chem. Res.* **1999**, *32*, 201.
(5) Finklea, H. O. In *Electroanalytical Chemistry*; Bard, A. J., Rubinstein, I., Eds.; Marcel Dekker: New York, 1996; Vol. 19, pp 109−335.
(6) Robinson, D. B.; Chidsey, E. D. *J. Phys. Chem.* **2002**, *106*, 10706.
(7) Sumner, J. J.; Creager, S. E. *J. Phys. Chem.* **2001**, *105*, 8739.
(8) Brevnov, D. A.; Finklea, H. O.; Van Ryswyk, H. *J. Electroanal. Chem.* 2001, *500*, 100−7.
(9) Smalley, J. F.; Finklea, H. O.; Chidsey, C. E. D.; Linford, M. R.; Creager, S. E.; Ferraris, J. P.; Chalfant, K.; Zawodzinsk, T.; Feldberg, S. W.; Newton, M. D. *J. Am. Chem. Soc.* **2003**, *125*, 2004.
(10) Hortholary, C.; Mine, F.; Coudret, C.; Bonvoisin, J.; Launay, J.-P. *Chem. Commun.* **2002**, 1932.
(11) Yamamoto, H.; Waldeck, D. H. *J. Phys. Chem.* **2002**, *106*, 7469.
(12) Sikes, H. D.; Smalley, J. F.; Dudek, S. P.; Cook, A. R.; Newton, M. D.; Chidsey, C. E. D.; Feldberg, S. W. *Science*. **2001**, *291*, 1519.
(13) Sek, S.; Bilewicz, R. *J. Electroanal. Chem.* **2001**, *509*, 11.
(14) Sumner, J. J.; Weber, K. S.; Hockett, L. A.; Creager, S. E. *J. Phys. Chem.* **2000**, *104*, 7449.
(15) Slowinski, K.; Chamberlain, R. V.; Miller, C. J.; Majda, M. *J. Am. Chem. Soc.* **1997**, *119*, 11910.
(16) Becka, A.; Miller, C. J. *J. Phys. Chem.* **1992**, *96*, 2657.
(17) Xu, Jie.; Li, H. L.; Zhang, Y. *J. Phys. Chem.* **1993**, *97*, 11497.
(18) Tender, L.; Carter, M. T.; Murray, R. W. *Anal. Chem.* **1994**, *66*, 3173.
(19) Paddon-Row, M. N. *Acc. Chem. Res.* **1994**, *27*, 18.
(20) Newton, M. D. *Chem. Rev.* **1991**, *91*, 767.
(21) Laviron, E. *J. Electroanal. Chem.* **1979**, *101*, 19.

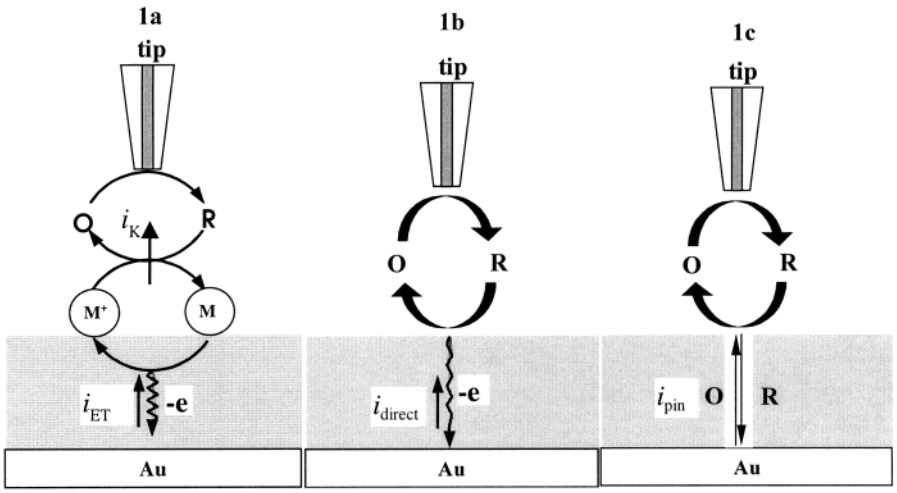

Figure 1. Schematic view of the processes involved in the SECM measurements of ET across an electroactive SAM: (a) mediated ET; (b) direct electron tunneling through monolayer; (c) ET through pinholes.

of the results and decrease the upper limit for the measurable rate constant. Recently, microelectrodes have been used to tackle this problem.[6,22] Generally, the electrochemical techniques can measure heterogeneous ET rate constants up to 10^7 s^{-1}.[6,9,12] More recently, temperature jump methods have been applied to these systems increasing the limit of ET rate constants to $\sim 10^8$ s^{-1}.[23]

SECM has the advantage that measurements are made at steady state, eliminating problems with double layer charging and other transient contributions such as oxide film formation and reduction. Moreover, the small size of the tip, and hence the measured currents, minimizes problems with resistive drop and allows very rapid mass transport to be attained, aiding in the measurement of fast reactions. SECM was previously used to study the adsorption kinetics of *n*-alkanethiols on gold[24] and menadione permeability through SAMs on gold.[25] Here, we develop new experimental and theoretical methodologies to measure the rates of ET reactions through molecular monolayers. Several different situations will be considered (Figure 1). The monolayer may contain redox centers (Figure 1a) or simply act as a blocking layer (Figure 1b). In Figure 1a, ET occurs via a bimolecular reaction between a dissolved redox species generated at the tip (R) and redox centers attached to the SAM (M^+) followed by the electron tunneling, while, in Figure 1b, it occurs by direct tunneling between the dissolved species, R, and the electrode. Finally, the charge transfer may occur through pinhole defects in the film (Figure 1c). Below, we demonstrate the possibility of measuring the rates of all of these processes and analyzing the combinations of different competing pathways for the long-distance ET. Our results indicate that, with a suitable redox mediator, the rates of both very fast bimolecular ET at the SAM/electrolyte interface and electron tunneling through the film can be measured. We note that Unwin and co-workers[26] used a transient SECM approach to measure the bimolecular ET between a solution species and bound ferrocene at the air/water interface.

(22) Weber, K.; Hockett, L.; Creager, S. E. *J. Phys. Chem. B.* **1997**, *101*, 8286.
(23) Feldberg, S. W.; Newton, M. D.; Smalley, J. F. In *Electroanalytical Chemistry*; Bard, A. J., Rubinstein, I., Eds.; Marcel Dekker: New York, 2003; Vol. 22, Chapter 2 (in press).
(24) Forouzan, F.; Bard, A. J.; Mirkin, M. V. *Isr. J. Chem.* **1997**, *37*, 155.
(25) Cannes, C.; Kanoufi, F.; Bard, A. J. *Langmuir* **2002**, *18*, 8134.
(26) Zhang, J.; Slevin, C. J.; Morton, C.; Scott, P.; Walton, D. J.; Unwin, P. R. *J. Phys. Chem. B* **2001**, *105*, 11120.

Theory

Mediated Electron Transfer. In this case, the monolayer adsorbed on the substrate contains an electroactive group, M, and the regeneration of the mediator occurs via a bimolecular reaction with these surface-bound redox centers (Figure 1a). In a typical SECM experiment, an oxidized form of a redox mediator is reduced at the tip electrode as shown in Figure 1 (equally, an oxidation reaction of the reduced form of the mediator can be used). The product of this reaction diffuses to the SAM/electrolyte interface where it reacts with the oxidized form of the monolayer-bound redox moieties (M^+):

$$R + M^+ \underset{k_{Red}}{\overset{k_{Ox}}{\rightleftharpoons}} O + M \qquad \text{(bimolecular ET at the film/solution interface)} \quad (1)$$

$$M - e \underset{k_f}{\overset{k_b}{\rightleftharpoons}} M^+ \qquad \text{(electron tunneling through the monolayer)} \quad (2)$$

The overall SECM process includes the following consecutive steps: (i) mass transfer in the tip/substrate gap (the diffusion limiting current for this step is given by eq 3);[27] (ii) bimolecular ET between the mediator species and the monolayer-bound redox centers [eq 1]; and (iii) the electron tunneling through the monolayer [eq 2]. The rates of steps (ii) and (iii) are given by eqs 4 and 5, respectively,

$$i_T^c = 4nFaDc^\circ\,(0.78377/L + 0.3315\exp(-1.0672/L) + 0.68) \quad (3)$$

$$i_K = nFA(k_{Ox}\Gamma_M{}^+ c_R^s - k_{Red}\Gamma_M c_O^s) \qquad \text{(quasi-reversible reaction)} \quad (4a)$$

or

$$i_K = nFAk_{Ox}\Gamma_M{}^+ c_R^s \qquad \text{(irreversible reaction)} \quad (4b)$$

$$i_{ET} = nFA(k_b\Gamma_M - k_f\Gamma_M{}^+) \qquad \text{(quasi-reversible reaction)} \quad (5)$$

(27) *Scanning Electrochemical Microscopy*; Bard, A. J., Mirkin, M. V., Eds.; Marcel Dekker: New York, 2001; pp 145−199.

where a is the tip radius, D and c° are the diffusion coefficient and bulk concentration of the redox mediator in solution, L is the normalized tip−substrate distance ($L = d/a$, where d is the distance between the tip and the substrate), A is the surface area, k_{Ox} and k_{Red} are the bimolecular oxidation−reduction rate constants (mol^{-1} cm^3 s^{-1}), k_b and k_f are the electron tunneling rate constants (s^{-1}), Γ_{M^+} and Γ_M are the surface concentrations (mol/cm^2) of oxidized and reduced forms of redox centers in the monolayer (the total coverage $\Gamma^* = \Gamma_M + \Gamma_{M^+}$), and c_R^s and c_O^s are the concentrations of reduced and oxidized forms of redox mediator at the substrate surface (mol/cm^3).

Reaction (1) is irreversible if $k_{Ox} \gg k_{Red}$ (i.e., $E^{\circ\prime}_{ads} \gg E^{\circ\prime}_{med}$, where $E^{\circ\prime}_{ads}$ and $E^{\circ\prime}_{med}$ are the formal potentials of the SAM-bound redox species and redox mediator in solution, respectively). This is the case in the present work. Reaction 1 is also irreversible when the substrate potential $E_S \gg E^{\circ\prime}_{ads}$ because in this case $\Gamma_{M^+} \gg \Gamma_M$. Therefore, one need only consider the combination of irreversible reaction 1 with either quasi-reversible or irreversible reaction 2.

Under steady-state conditions, i_K must be equal to i_{ET}. Thus,

$$k_{Ox}\Gamma_{M^+}c_R^s = k_b\Gamma_M - k_f\Gamma_{M^+} = k_b(\Gamma^* - \Gamma_{M^+}) - k_f\Gamma_{M^+} \quad (6)$$

from which one can obtain

$$\Gamma_{M^+} = k_b\Gamma^*/(k_{Ox}c_R^s + k_b + k_f) \quad (7)$$

and

$$i_K = i_{ET} = nFAk_{Ox}c_R^s k_b\Gamma^*/(k_{Ox}c_R^s + k_b + k_f) \quad (8)$$

Therefore, the characteristic (limiting) current representing the combination of reactions 1 and 2 is

$$i_e = nFAk_{Ox}c^\circ k_b\Gamma^*/(k_{Ox}c^\circ + k_b + k_f) \quad (9)$$

As discussed previously,[28] the reciprocal of the substrate current (i_S) under steady-state conditions can be written as

$$1/i_S = 1/i_T^c + 1/i_e \quad (10)$$

Substituting eq 9 into eq 10 yields

$$1/i_S = 1/i_T^c + 1/nFAk_b\Gamma^* + (1 + k_f/k_b)/nFAk_Oc^\circ\Gamma^* = 1/i_T^c + 1/i_{ET}^{lim} + (1 + k_f/k_b)/i_K^{lim} \quad (11)$$

where i_K^{lim} and i_{ET}^{lim} are the characteristic currents of reactions 1 and 2, respectively. Equation 11 is very similar to an equation used in ref 29 for quasi-reversible charge transfer coupled with diffusion to a uniformly accessible electrode.

Equation 10 is equivalent to eq 9 in ref 28. Comparing these equations, one can see that the effective rate constant obtained by fitting an experimental approach curve to theory (i.e., eq 6 in ref 28) should be equal to

$$k_{eff} = k_{Ox}k_b\Gamma^*/(k_{Ox}c^\circ + k_b + k_f) \quad (12)$$

(28) Wei, C.; Bard, A. J.; Mirkin, M. V. *J. Phys. Chem.* **1995**, *99*, 16033.
(29) Mirkin, M. V.; Bard, A. J. *Anal. Chem.* **1992**, *64*, 2293.

There are two limiting cases: (a) $k_{Ox}c^\circ \gg k_b + k_f$ (i.e., $E^{\circ\prime}_{ads} \gg E^{\circ\prime}_{med}$, c° is not very small, and E_S is not much more positive than $E^{\circ\prime}_{ads}$). Under these conditions, eq 12 is reduced to

$$k_{eff} \cong k_b\Gamma^*/c^\circ \quad (13)$$

and the k_b value can be extracted from the slope of the linear dependence of k_{eff} vs $1/c^\circ$.

One should notice that the effective rate constant in eq 13 is inversely proportional to c°; i.e., the higher the bulk concentration of the mediator, the faster the rate constants that can be measured. Since the steady-state tip current is essentially unaffected by iR-drop and migration effects, one can do experiments with a very high mediator concentration (e.g., $\geq 10^{-4}$ mol/cm^3).

(b) $k_{Ox}c^\circ \ll k_b + k_f$ (i.e, either $E^{\circ\prime}_{ads} \approx E^{\circ\prime}_{med}$ and c° is small or $E_S \gg E^{\circ\prime}_{ads}$). In this case, eq 12 becomes

$$k_{eff} \cong k_{Ox}k_b\Gamma^*/(k_b + k_f) \quad (14)$$

so that k_{eff} is concentration independent. Moreover, if $E_S \gg E^{\circ\prime}_{ads}$,

$$k_{eff} \cong k_{Ox}k_b\Gamma^*/k_b = k_{Ox}\Gamma^* \quad (15)$$

i.e., k_{eff} is also potential-independent, and the k_{Ox} value can be obtained from eq 15.

The upper limits for the k_b and k_{Ox} that can be measured with SECM can be estimated as follows. When the tip is very close to the substrate (i.e., $L \ll 1$), the mass transfer coefficient $m_o \approx D/d$, and the upper limit for measurable k_{eff} is $\sim 5m_o = 5D/d$.[27] The tip can be brought down to $L \approx 0.1$. Thus, for a 1-μm radius tip, $d = 10^{-5}$ cm. Assuming a typical diffusion coefficient $D = 10^{-5}$ cm^2/s, $\Gamma^* \approx 10^{-11}$ mol/cm^2 and $c^\circ = 2 \times 10^{-4}$ mol/cm^3, from eq 13 the upper limit for measurable k_b is $\sim 10^8$ s^{-1}. Similarly, to measure k_{Ox}, i_K should be of the order or lower than i_T; i.e., $nFAk_{Ox}\Gamma^*c^\circ < nFADc^\circ/d$, which results in $k_{Ox} < D/d\Gamma^*$. Thus, with $D = 10^{-5}$ cm^2/s, $\Gamma^* \approx 2 \times 10^{-12}$ mol/cm^2, and $d = 10^{-5}$ cm (for a 1-μm radius tip), the upper limit for measurable k_{Ox} is 5×10^{11} mol^{-1} cm^3 s^{-1} (or 10^8 M^{-1} s^{-1}).

Direct Electron Tunneling Through the Monolayer. When the monolayer is blocking (i.e., it contains no redox centers capable of reacting with the mediator species), the mediator regeneration can occur via direct tunneling through the film (Figure 1b). The characteristic current for this reaction is

$$i_{direct} = nFAk_{direct}c^\circ \quad (16)$$

where k_{direct} is the rate constant of direct electron tunneling.

In the presence of pinhole defects in a blocking monolayer, these provide an additional pathway for ET (Figure 1c) with a characteristic current

$$i_{pin} = nFA''k_{pin}c^\circ \quad (17)$$

where k_{pin} is the rate constant of the ET through pinholes, $A'' = A \times \theta_{pin}$ and θ_{pin} is the fractional area of the pinholes in the SAM.

The reactions in Figure 1b and c occur in parallel, so the total current through the film is the sum of two terms

$$i_{e,total} = i_{direct} + i_{pin} \quad (18)$$

and the effective rate constant, which can be obtained by fitting an experimental approach curve to theory (i.e., eq 6 in ref 28) reflects the contributions of both pathways:

$$k_{\text{eff}} = k_{\text{direct}} + \theta_{\text{pin}}\, k_{\text{pin}} \tag{19}$$

Combination of Mediated ET and Direct Tunneling. If an SAM is composed of a mixture of electroactive and nonelectroactive components, all three pathways discussed above can contribute to the ET through the film. The total current across the monolayer in this case is

$$i_{\text{e,total}} = i_{\text{e}} + i_{\text{direc}} + i_{\text{pin}} \tag{20}$$

where $i_{\text{direc}} = nFA'k_{\text{direct}}\, c^{\circ}$, $A' = A(1 - \theta_{\text{M}})$, and θ_{M} is the fraction of the substrate surface covered by redox centers; i_{e} and i_{pin} are given by eqs 9 and 17, respectively.

Correspondingly, eqs 10 and 12 should modified as follows:

$$1/i_{\text{S}} = 1/i_{\text{T}}{}^{\text{c}} + 1/i_{\text{e,total}} \tag{21}$$

$$k_{\text{eff}} = [k_{\text{Ox}}k_{\text{b}}\Gamma^*/(k_{\text{Ox}}c^{\circ} + k_{\text{b}} + k_{\text{f}})] + k' \tag{22}$$

where $k' = (1 - \theta_{\text{M}})k_{\text{direct}} + \theta_{\text{pin}}k_{\text{pin}}$. k' represents the contribution from direct tunneling and ET through defects.

As discussed above, there are two limiting cases: (a) $k_{\text{Ox}}c^{\circ} \gg k_{\text{b}} + k_{\text{f}}$, which yields

$$k_{\text{eff}} \cong (k_{\text{b}}\Gamma^*/c^{\circ}) + k' \tag{23}$$

Despite the direct tunneling effect, the plot of k_{eff} vs $1/c^{\circ}$ is linear, and the k_{b} value can be extracted from its slope. The nonzero intercept of the k_{eff} vs $1/c^{\circ}$ dependence gives the k' value.

(b) $k_{\text{Ox}}c^{\circ} \ll k_{\text{b}} + k_{\text{f}}$, when k_{eff} becomes concentration independent

$$k_{\text{eff}} \cong [k_{\text{Ox}}k_{\text{b}}\Gamma^*/(k_{\text{b}} + k_{\text{f}})] + k' \tag{24}$$

Moreover, if $E_{\text{S}} \gg E^{\circ\prime}_{\text{ads}}$,

$$k_{\text{eff}} \cong [k_{\text{Ox}}k_{\text{b}}\Gamma^*/k_{\text{b}}] + k' = k_{\text{Ox}}\Gamma^* + k' \tag{25}$$

Thus, the k_{Ox} value can be obtained from the slope of the k_{eff} vs Γ^*plot.

There are two implicit assumptions that can lower the accuracy of the above analysis. First, it is assumed that c_R^S is the same across the portion of substrate surface facing the tip (i.e., a uniformly accessible substrate). Second, Γ_{M} and Γ_{M^+} are assumed to be uniform for the same portion of the substrate surface. Both assumptions should be more accurate at small L and less accurate at large distances.

Experimental Section

Chemicals. *n*-Alkyl thiols ($CH_3(CH_2)_nSH$, where $n = 5,7, 8, 9,$ and 14) and sodium perchlorate were purchased from Aldrich (Milwaukee, WI). Dodecanethiol was from Sigma Chemical Co. (St. Louis, MO), and tetradecanethiol was purchased from Lancaster Synthesis Inc (Windham, NH). Hexaammineruthenium chloride and sodium hexachloroiridate were purchased from Strem Chemicals (Newburyport, MA) and used as received. The ferrocenyl-alkanethiols containing ester bonds were a gift from C. E. D. Chidsey (Department of Chemistry, Stanford University), and the ferrocenyl-alkanethiols containing amide bonds were provided by S. E. Creager (Department of Chemistry, Clemson University). Ethanol was absolute analytical grade. All solutions were prepared with deionized water (Milli-Q, Millipore Corp.).

Monolayer Deposition. Thiol monolayers were assembled onto the evaporated gold electrodes. The Au substrates were prepared by thermal evaporation of chromium followed by gold (99.99% purity) onto a glass slide at approximately 1×10^{-6} Torr. The thickness of the chromium and gold films were typically 30 and 1500−2000 Å, respectively. After cleaning in hot 1:3 H_2O_2 (30%)/H_2SO_4 (CAUTION! THIS SOLUTION IS A VERY STRONG OXIDIZING AGENT AND VERY DANGEROUS TO HANDLE IN THE LABORATORY. PROTECTIVE EQUIPMENT INCLUDING GLOVES, GOGGLES, AND FACE SHIELDS SHOUD BE USED AT ALL TIMES) and rinsing with water, the gold substrates were electrochemically cleaned by cycling over the range −0.3 to 1.5 V vs Ag/AgCl in 0.5 M H_2SO_4 until reproducible CVs were obtained. The electrode was then rinsed with water and absolute ethanol, dried in a stream of pure argon, and immersed in an ethanol solution containing thiols. For monolayers containing only nonelectroactive thiols, the coating solutions were typically 20 mM in thiol, and the gold surface was exposed to this coating solution for at least 48 h. Mixed monolayers containing long-chain ferrocenyl-thiols were prepared by soaking the gold substrates in 1 mM ferrocenyl-thiol ($FcCO_2(CH_2)_{16}SH$ or $FcCONH(CH_2)_{15}SH$) and 9 mM diluent thiol (e.g., $CH_3(CH_2)_{14}SH$) for at least 48 h. Mixed monolayers containing short-chain ferrocenyl-thiols were prepared by soaking the gold substrates in 0.5 mM $FcCONH(CH_2)_7SH$ and 0.5 mM $CH_3(CH_2)_8SH$ for 1 day, followed by placing the electrodes in a second coating solution containing 20 mM $CH_3(CH_2)_8SH$ for 1 week. Before SECM measurements, the electrode was rinsed with absolute ethanol and deionized water and dried in a stream of argon.

SECM Instrumentation and Procedure. Electrochemical experiments were carried out using a CHI-900 scanning electrochemical microscope (CH Instruments, Austin, TX), employing a three-electrode cell: the gold electrode acted as the working electrode, a platinum wire as the counter electrode, and an Ag/AgCl wire in 3 M KCl as the reference electrode. All potentials are reported with respect to this reference. The SECM approach curves were obtained with a 2-, 5-, or 25-μm diameter Pt or a 25-μm diameter Au tip. The RG values of the tips used in this work were about 5. These tips were polished with 0.05-μm alumina before each experiment. The gold substrate was attached to the bottom of the Teflon cell using an O-ring. The solution was purged with argon before measurements.

The positioning of the tip was carried out by recording the approach curve. The electrochemical cell was mounted on an adjustable platform to compensate for any substrate tilt. The tip was first laterally scanned until it was located above the center of the substrate and then moved to the substrate surface. The approach curve showing feedback was then recorded, and the coordinate of the substrate/solution interface ($d = 0$) was determined from the sharp change of the tip current that occurred when the tip just touched the substrate surface. Each data point shown in the figures represents the average of three measurements made with a tip approaching different parts of the substrate surface.

Results and Discussion

Blocking Properties of Electroactive and Nonelectroactive SAMs. The voltammogram of a ferrocene-terminated monolayer on gold (Figure 2) reveals the characteristics expected for a reversible ET between immobilized redox species and electrode surface, i.e., symmetric waves and small separation between anodic and cathodic peak potentials. Within the potential range where no ferrocene oxidation occurs, ferrocene-terminated alkanethiol monolayers were blocking the ET between dissolved redox species ($Ru(NH_3)_6{}^{3+}$) and the underlying Au. Figure 3 shows that the blocking effect of a mixed long-chain monolayer ($FcCONH(CH_2)_{15}SH/CH_3(CH)_{14}SH$) was very similar to that produced by a nonelectroactive thiol ($CH_3(CH)_{14}SH$) film.

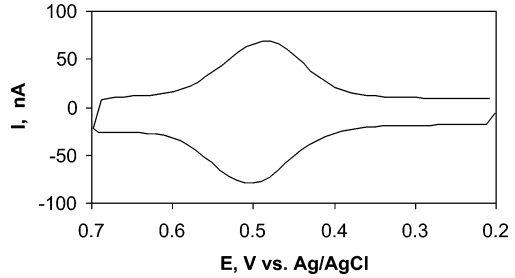

Figure 2. Cyclic voltammogram of a mixed monolayer of $FcCONH(CH_2)_{15}SH$ and $CH_3(CH)_{14}SH$ in a solution containing 0.1 mM $Ru(NH_3)_6Cl_3$ and 0.1 M $HClO_4$. The potential scan rate was 100 mV/s.

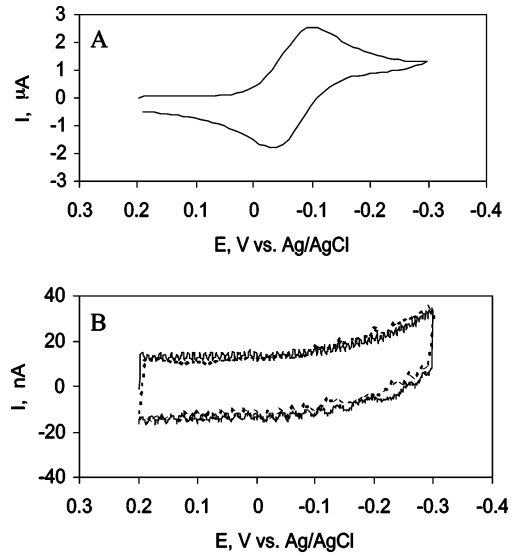

Figure 3. Cyclic voltammograms of 0.1 mM $Ru(NH_3)_6Cl_3$ at (A) bare gold and (B) gold coated with a mixed $FcCONH(CH_2)_{15}SH/CH_3(CH)_{14}SH$ monolayer (solid line) and with a monolayer of $CH_3(CH)_{14}SH$ (dashed line). The area of the Au substrate was 0.096 cm^2. Solution contained 0.1 M $HClO_4$. The potential scan rate was 100 mV/s.

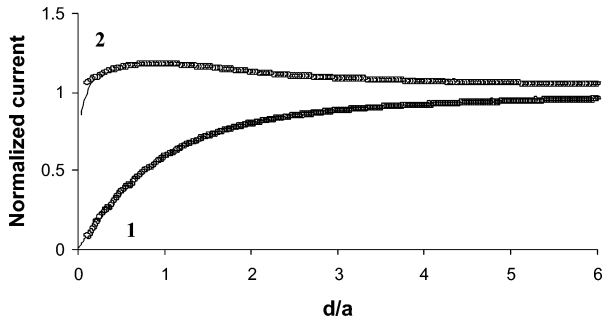

Figure 4. SECM approach curves obtained at a gold substrate coated with a mixed monolayer of $FcCONH(CH_2)_{15}SH$ and $CH_3(CH)_{14}SH$ in solution containing 0.1 mM $Ru(NH_3)_6Cl_3$ and 0.1 M $HClO_4$. The tip was a 12.5-μm radius Au disk held at −0.2 V vs Ag/AgCl. Substrate potential was (1) 0.2 and (2) 0.5 V vs Ag/AgCl. The tip scan rate was 1 μm/s. The solid lines are theoretical SECM curves.

The excellent blocking characteristics of long-chain monolayers were confirmed by SECM measurements. Figure 4 shows the current−distance curves for a 25-μm diameter Au tip held at −0.2 V approaching a gold substrate coated with the mixed long-chain monolayer and immersed in a 0.1 mM $Ru(NH_3)_6Cl_3$ solution (generating $(Ru(NH_3)_6^{2+})$. When the substrate potential, E_{sub}, was kept at 0.2 V (Figure 4, curve 1), which is far positive of the formal potential of the ruthenium couple ($E^{o\prime} = -0.10$ vs Ag/AgCl), but where the ferrocene redox centers

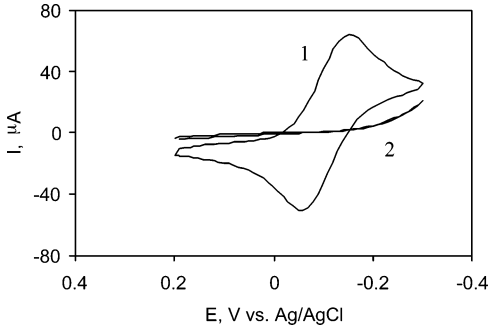

Figure 5. Cyclic voltammograms of 1 mM $Ru(NH_3)_6Cl_3$ at (1) bare gold and (2) gold coated with a mixed monolayer of $FcCONH(CH_2)_7SH$ and $CH_3(CH)_8SH$. Solution contained 0.05 M $NaClO_4$. The area of the Au electrode was 0.38 cm^2. The potential scan rate was 100 mV/s.

remain in the reduced form, the feedback current could only be attributed to direct electron tunneling (i.e., ET through the monolayer between $Ru(NH_3)_6^{2+}$ and Au) and by ET through pinholes. The feedback current at this potential was so low that the approach curve fits the theory for an insulating substrate (curve 1 in Figure 4). Thus the k' value (i.e., the sum of the rate constants of direct electron tunneling and ET through pinholes in eq 22) was too low to measure under these experimental conditions. This result is consistent with earlier studies of the good blocking properties of long-chain alkylthiol monolayers,[5,30,31] which showed that annealed long ($n \geq 11$) alkyl chain assemblies are densely packed, essentially pinhole-free, and act as effective ET barriers. These studies also ruled out the possibility that hydrophilic redox species can penetrate through the monolayer and react at the electrode surface.

Curve 2 in Figure 4 was obtained at $E_{sub} = 0.5$ V, where the oxidation of ferrocene occurs. At this potential, the SECM approach curves obtained at a nonelectroactive ($CH_3(CH)_{14}SH$) monolayer were similar to curve 1 (not shown). Thus, the regeneration of $Ru(NH_3)_6^{3+}$ via direct electron tunneling or through ET at pinholes and defects was very slow even at $E_{sub} = 0.5$ V. The much larger SECM feedback current obtained at the ferrocene-terminated monolayer (Figure 4, curve 2) was produced almost entirely by the bimolecular ET pathway (eqs 1 and 2), since the mixed monolayer and the monolayer composed only of diluent thiol exert similar blocking effects on direct electron tunneling (see Figure 3b).

Figure 5 shows a voltammogram of $Ru(NH_3)_6^{3+}$ at a gold electrode coated with a shorter-chain mixed monolayer, $FcCONH(CH_2)_7SH/CH_3(CH)_8SH$. As expected, the cathodic current at the short-chain SAM was higher than that obtained with a long-chain monolayer (cf. Figure 3) (note the difference in the substrate areas and the mediator concentrations) (note difference in current scales in Figures 3B and 5, curve 2). The voltammogram of a monolayer composed only of diluent thiol ($CH_3(CH)_8SH$) was identical to curve 2 in Figure 5. The result again suggests that ET to the mediator was effectively blocked by both the mixed monolayer and the nonelectroactive monolayer SAM. The well-ordered structure of shorter-chain electroactive SAMs was also found in the study of electron tunneling across monolayers with attached ruthenium(II/III) redox centers,[32] which are close-packed as long as the redox centers are

(30) Porter, M. D.; Bright, T. B.; Allara, D. L.; Chidsey, A. E. D. *J. Am. Chem. Soc.* **1987**, *109*, 3559.
(31) Slowinski, K.; Chamberlain, R. V.; Miller, C. J.; Majda, M. *J. Am. Chem. Soc.* **1997**, *119*, 11910.

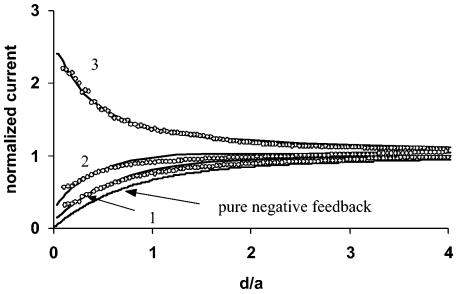

Figure 6. SECM approach curves obtained on gold coated by a mixed monolayer of $FcCONH(CH_2)_7SH$ and $CH_3(CH)_8SH$ in a solution containing 1 mM $Ru(NH_3)_6Cl_3$ and 0.05 M $NaClO_4$ (pH 3). The tip was a 1-μm radius Pt disk. Substrate potential was (1) 0.2 and (2,3) 0.5 V vs Ag/AgCl. Curve 2 was obtained on the monolayer of $CH_3(CH)_8SH$. The approaching speed was 0.2 μm/s. The solid lines are theoretical SECM curves.

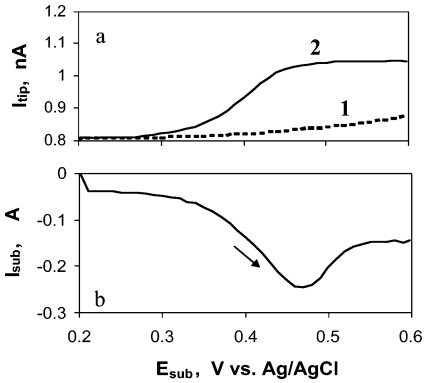

Figure 7. Dependences of the tip (a) and substrate (b) current on substrate potential. The tip was a 5-μm diameter Pt disk. The Au substrate was coated with a mixed monolayer of $FcCONH(CH_2)_7SH$ and $CH_3(CH_2)_8SH$ (solid lines) or a monolayer composed only of $CH_3(CH_2)_8SH$ (dashed line). The solution contained 1 mM $Ru(NH_3)_6Cl_3$ and 0.05 M $NaClO_4$ (pH 3). The tip potential was -0.26 V vs Ag/AgCl. The distance between the tip and the substrate was $\sim$5 mm. The potential scan rate was 100 mV/s.

not deeply buried into the film (i.e., the diluent chain is not more than two methylenes longer than the redox chain).

Figure 6 shows the SECM approach curves obtained with the shorter-chain monolayers (both electroactive and nonelectroactive). At $E_{sub} = 0.2$ V, the current−distance curves obtained at Au coated with either $FcCONH(CH_2)_7SH/CH_3(CH)_8SH$ or $CH_3(CH)_8SH$ (Figure 6, curve 1) were similar to the theoretical curve for the pure negative feedback (solid line). Therefore, within the potential range where the ferrocene groups remain reduced, the blocking properties of electroactive and nonelectroactive C_9 SAMs are very similar. At $E_{sub} = 0.5$ V, a measurable feedback current was observed at the monolayer of only diluent thiol (Figure 6, curve 2), implying that the regeneration of $Ru(NH_3)_6^{3+}$ through direct electron tunneling or through ET at pinholes cannot be neglected at more positive potentials with the shorter chain thiols. The much higher feedback current observed at the ferrocene-terminated monolayer at $E_{sub} = 0.5$ V (Figure 6, curve 3), however, indicates that the mediated ET (eqs 1 and 2) is the dominant mediator regeneration pathway under these conditions. The relative significance of the contributions of direct tunneling and bimolecular ET can be better understood from the dependence of the tip current on substrate potential (Figure 7). These curves were obtained with a tip positioned at an $\sim$5-μm distance from the substrate. The

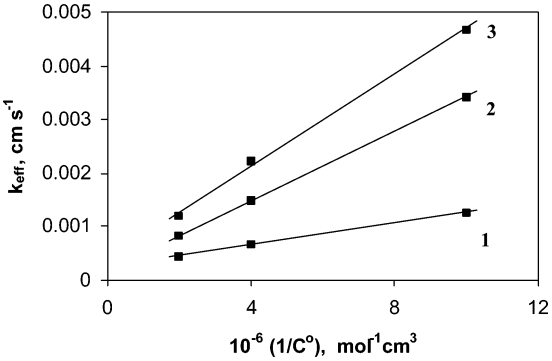

Figure 8. Dependence of the effective heterogeneous rate constant on the concentration of an $Ru(NH_3)_6Cl_3$ mediator measured with a mixed $FcCONH(CH_2)_{15}SH/CH_3(CH)_{15}SH$ monolayer in solution containing 0.1 M $HClO_4$. The tip was a 12.5-μm radius Au disk with $E_{tip} = -0.2$ V and $E_{sub} =$ (1) 0.5, (2) 0.55, and (3) 0.58 V vs Ag/AgCl. $\Gamma^* = 3.0 \times 10^{-12}$ mol cm^{-2}.

tip potential was kept at a sufficiently negative value to reduce the $Ru(NH_3)_6^{3+}$ mediator at a diffusion-controlled rate, and both the tip and the substrate currents were recorded as a function of substrate potential. Curve 1 in Figure 7a was obtained with a monolayer composed only of diluent thiol $CH_3(CH_2)_8SH$, while curve 2 corresponds to a mixed $FcCONH(CH_2)_7SH/CH_3(CH_2)_8SH$ monolayer. Clearly, the difference between the feedback currents obtained at the nonelectroactive and electroactive SAMs increases over the substrate potential range from $\sim$0.3 V to $\sim$0.45 V, where ferrocene groups are oxidized (Figure 7b). This difference reflects the contribution of the mediated ET to the feedback current. Clearly, at $E_{sub} \geq \sim$0.45 V, ferrocene-mediated ET becomes the dominant pathway of the mediator regeneration.

ET Rate between the Underlying Metal and Redox Centers Attached to an SAM. The rate of long-distance ET across the mixed SAMs containing ferrocenyl-thiols was measured using $Ru(NH_3)_6^{3+}$ as the mediator in solution. The k_{Ox} of the bimolecular ET between $Ru(NH_3)_6^{2+}$ and the monolayer-bound ferrocenium was found to be $>10^{10}$ mol^{-1} cm^3 s^{-1}(see below). Using the ET rate constants measured previously for $FcCOO(CH_2)_{16}SH$[33] and $FcCONH(CH_2)_{15}SH$[34] monolayers on gold (1.3 s^{-1} and 7.0 s^{-1}, respectively) as an estimate for the k_b, one can expect the condition $k_{Ox}c^\circ \gg k_b + k_f$ to be fulfilled for $c^\circ \approx 10^{-6}$ mol/cm^3. Thus, eq 23 can be used to extract the k_b value from the experimental approach curves. The linear k_{eff} vs $1/c^\circ$ or k_{eff} vs Γ^*dependences (Figures 8 and 9) obtained for the long-chain mixed monolayers confirmed the validity of eq 23. These dependences were used to extract the k_b for different values of the substrate potential.

The standard ET rate constant, k°, was derived from the Butler−Volmer equation for the adsorbed reactant:

$$k_f = k^\circ \exp[-\alpha F(E_S - E^{\circ\prime}_{ads})/RT] \quad (26a)$$

$$k_b = k^\circ \exp[(1-\alpha)F(E_S - E^{\circ\prime}_{ads})/RT] \quad (26b)$$

where α is the transfer coefficient, F is the faradaic constant, R is the gas constant, and T is temperature.

The k° values obtained for different ferrocene monolayers are collected in Table 1. α was assumed to be 0.5 in the

(32) Finklea, H. O.; Liu, L.; Ravenscroft, M. S.; Punturi, S. *J. Phys. Chem.* **1996**, *100*, 18852.
(33) Chidsey, C. E. D. *Science*, **1991**, *251*, 919.
(34) Weber, K.; Creager, S. E. *Anal. Chem.* **1994**, *66*, 3164.

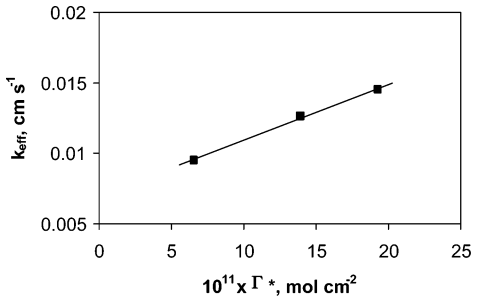

Figure 9. Dependence of the effective heterogeneous rate constant on the coverage of ferrocene measured with a mixed $FcCOO(CH_2)_{16}SH/CH_3(CH)_{13}SH$ monolayer in solution containing 1 mM $Ru(NH_3)_6Cl_3$ and 0.1 M $HClO_4$. The tip was a 12.5-μm radius Au disk with $E_{tip} = -0.2$ V and $E_{sub} = 0.8$ V vs Ag/AgCl.

Table 1. Standard ET Rate Constants for Ferrocene Monolayers

redox thiol	diluent thiol	mediator	$k°$, s^{-1}
$FcCONHC_{15}SH$	$C_{15}SH$	$Ru(NH_3)_6^{3+}$	7.0 ± 0.4
$FcCONHC_{15}SH$	$C_{16}SH$	$Ru(NH_3)_6^{3+}$	20 ± 1
$FcCOOC_{16}SH$	$C_{14}SH$	$Ru(NH_3)_6^{3+}$	2.4 ± 0.2
$FcCONHC_{15}SH$	$C_{15}SH$	$IrCl^{3-}$	12 ± 1
$FcCONHC_7SH$	C_9SH	$Ru(NH_3)_6^{3+}$	$(1.2 \pm 0.1) \times 10^5$

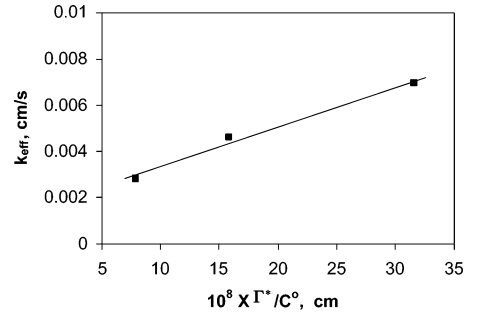

Figure 10. Dependence of the effective heterogeneous rate constant on the concentration of Na_3IrCl_6 measured with an $FcCONH(CH_2)_{15}SH/CH_3(CH)_{14}SH$ monolayer in solution containing 0.1 M $HClO_4$. The tip was a 12.5-μm radius Au disk. $E_{sub} = 0$ V vs Ag/AgCl.

calculation of $k°$ values. In some additional experiments, the mediator was $IrCl_6^{3-}$, which was oxidized at the tip and rereduced by the monolayer-bound ferrocene. The substrate in these experiments was biased at a more negative potential (e.g., 0 V), and the measured rate constants (k_f) corresponded to the ET from Au to the ferrocenium moieties. Since the condition $k_{Red}c° \gg k_b + k_f$ is fulfilled in this case, the k_f values were extracted from the linear k_{eff} vs $\Gamma*/c°$ dependences (Figure 10). Importantly, the standard rate constant values found by measuring the forward and reverse long-distance ET rates with different dissolved redox species are in a good agreement with each other.

The k' values obtained from the intercepts in Figures 8 and 10 were 4.1×10^{-4} and 1.7×10^{-3} cm/s, respectively. These numbers are very close to the k_{eff} values obtained for the corresponding nonelectroactive monolayer ($C_{15}SH$) at the same substrate potential, i.e., 3.7×10^{-4} and 1.0×10^{-3} cm/s for mediator $Ru(NH_3)_6^{3+}$ and $IrCl_6^{3-}$, respectively. Therefore, the contributions of the direct electron tunneling and ET through pinholes to the measured rate constant can be evaluated by measuring the k_{eff} at the corresponding nonelectroactive SAMs. This approach was used to measure the rates of ET across short-chain ferrocenyl-thiol SAMs ($FcCONH(CH_2)_7SH$). For such monolayers, the condition $k_{Ox}c° \gg k_b + k_f$ does not hold because

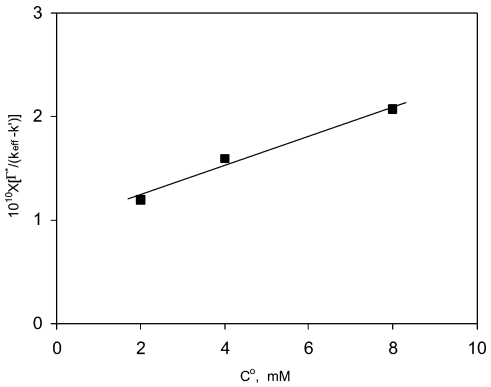

Figure 11. Dependence of the effective heterogeneous rate constant on the concentration of $Ru(NH_3)_6Cl_3$ measured for a shorter-chain mixed monolayer ($FcCONH(CH_2)_7SH/CH_3(CH)_8SH$) in a 0.05 M $NaClO_4$ solution. The tip was a 1-μm radius Pt disk. The substrate potential was 0.5 V vs Ag/AgCl.

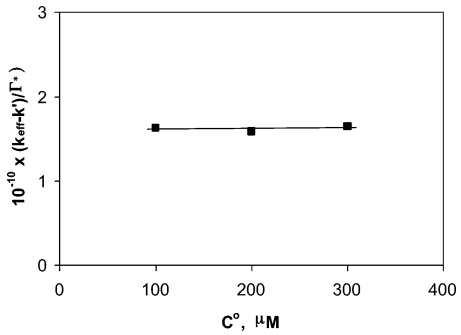

Figure 12. Dependence of the effective heterogeneous rate constant on the concentration of an Na_3IrCl_6 mediator measured with a mixed monolayer of $FcCONH(CH_2)_{15}SH/CH_3(CH)_{14}SH$. Solution contained 0.1 M $HClO_4$. The tip was a 2.5-μm radius Au disk. The substrate potential was 0 V vs Ag/AgCl.

of a much larger $k°$ ($\sim 10^5$ s^{-1} for $FcCONH(CH_2)_7SH$[14]), and the general eq 22 has to be used instead of eq 23 to extract the rate constants. Equation 22 can be rewritten as

$$\frac{\Gamma*}{k_{eff} - k'} = \frac{c°}{k_b} + \frac{1 + \exp[-F(E_S - E_{ads}^{\circ\prime})/RT]}{k_{Ox}} \qquad (27)$$

Figure 11 shows the corresponding plot obtained for an $FcCONH(CH_2)_7SH/CH_3(CH)_8SH$ monolayer. Assuming $\alpha = 0.5$, the $k°$ value calculated from the slope of the straight line (1.2×10^5 s^{-1}) is close to those measured previously by cyclic voltammetry (6.6×10^4)[22] and ac voltammetry (1.1×10^5 s^{-1}).[14]

Bimolecular ET between the Monolayer-Bound Redox Centers and Redox Species in Solution. If $k_{Red}c° \ll k_b + k_f$ and $E_S \ll E_{ads}^{\circ\prime}$, an equation analogous to eq 25 can be used to extract the rate constants of the bimolecular ET:

$$k_{eff} = k_{Red}\Gamma* + k' \qquad (28)$$

With a small (sub-mM) concentration of $IrCl_6^{3-}$ in solution and a sufficiently negative substrate potential, both conditions were fulfilled, and k_{eff} became concentration independent (Figure 12). The k' value (1.7×10^{-3} cm/s) obtained from Figure 10 was used in plotting Figure 12. The rate constant of ET between bound ferrocene and $IrCl_6^{2-}$ was calculated to be $k_{Red} = 1.6 \times 10^{10}$ mol^{-1} cm^3 s^{-1}.

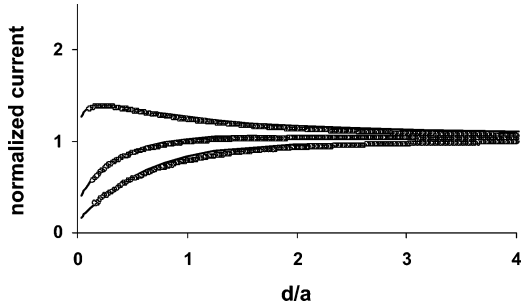

Figure 13. SECM approach curves obtained at an Au substrate coated by an HSC_{12} SAM with its potential held at (from top to bottom) 0.6, 0.4, and 0.2 V vs Ag/AgCl. The tip was a 12.5-μm radius Au disk biased at −0.2 V. Solution contained 1 mM $Ru(NH_3)_6Cl_3$ and 0.1 M $HClO_4$. The solid lines are theoretical SECM curves.

This result can be compared to the theoretical value found from the Marcus formula:[35]

$$k_{12} = (k_{11}k_{22}K_{12}f)^{1/2} \quad (29)$$

where k_{11} and k_{22} are the self-exchange rate constants for the two redox couples, $K_{12} = \exp(-nF\Delta E°/RT)$ is the equilibrium constant for the reaction (in solution) $IrCl_6^{2-} + Fc \rightleftarrows IrCl_6^{3-} + Fc^+$, $\Delta E°$ is the difference between the two standard potentials, and $\log f = (\log K_{12})^2/(4 \log(k_{11}k_{22}/Z_{soln}^2))$, and Z_{soln} is the collision frequency ($f \approx 1$ is typically assumed). The self-exchange rate constants for $IrCl_6^{3-/2-}$ and ferrocene are 2.5×10^8 [36] and 10^{10} mol^{-1} cm^3 s^{-1},[37] respectively. The substitution of these values in eq 29 yields $k_{12} = 3 \times 10^{11}$ mol^{-1} cm^3 s^{-1}, which is somewhat higher than our experimental value.

The value of k_{Ox} for ET between bound ferrocene and $Ru(NH_3)_6^{3+}$ in solution was found to be $\geq 4.5 \times 10^{10}$ mol^{-1} cm^3 s^{-1}. The k_{Ox} value was obtained using eq 27 based on the data shown in Figure 11. The theoretical k_{Ox} value calculated using eq 29 is 10^{13} mol^{-1} cm^3 s^{-1} [$k_{11}(Ru(NH_3)_6^{2+/3+}) = 3 \times 10^3$ mol^{-1} cm^3 s^{-1}].[38]

The discrepancy is likely due to the difference in the reactivities of the bound ferrocene and that freely diffusing in solution. These observations are qualitatively consistent with the results of Zhang et al.[26] who measured the rate constant of electron transfer between the solution mediator and an air/water monolayer-bound species via feedback mode transient measurements. However their measured values were orders of magnitude smaller than those predicted by Marcus theory.

ET across Electroinactive Monolayers. In this case, the mediator is regenerated by direct electron tunneling through the monolayer between an electrode and a freely diffusing redox probe (Figure 1b), assuming that the density of pinholes and other defects is low. The k_{direct} was obtained by fitting the SECM approach curves to theory. Figure 13 shows the approach curves obtained at a gold substrate coated with a $CH_3(CH)_{12}SH$ thiol monolayer with $Ru(NH_3)_6^{3+}$ as the mediator. The rate constant measured for alkanethiols with different chain lengths obtained at the same overpotential decreases exponentially with the number of methylene groups in the spacer molecule (Figure 14). The tunneling decay constant, β, obtained from the slope is 1.0 per methylene group. This value is in good agreement with earlier reports in which other nontethered redox molecules were employed.[13,16,17,31] The β-values of 1.02 ± 0.20 and 1.08 ± 0.20 per methylene group were obtained for alkanethiolate[17] and ω-hydroxyalkanthiolate[16] monolayers on gold electrodes, from voltammetry of $Fe(CN)_6^{3}$, $W(CN)_8^{3-}$, $Mo(CN)_8^{3-}$, and $Fe(bpy)(CN)_4^-$ redox species in aqueous solutions. For alkanethiolate and ω-hydroxyalkanthiolate monolayers on mercury electrodes, the value of β was determined to be 1.14 per CH_2, using $Ru(NH_3)_6^{3+}$ as the redox probe.[31]

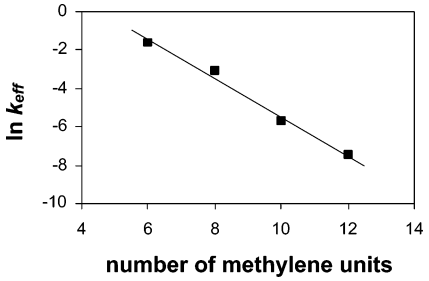

Figure 14. Dependence of ln k_{eff} on the number of methylene units in alkanethiols ($CH_3(CH_2)nSH$, where n = 5, 7, 9, and 11) in a solution containing 1 mM $Ru(NH_3)_6Cl_3$ and 0.1 M $HClO_4$. The substrate potential was held at 0.6 V vs Ag/AgCl.

Conclusions

New methodologies were developed and used to investigate long-distance ET across molecular monolayers by SECM. Rate constants were measured for electron tunneling through long-chain and short-chain alkanethiol SAMs between the gold electrode and redox species either covalently attached to the monolayer or freely diffusing in solution. From the same set of data, one also can determine a bimolecular rate constant for ET between the monolayer-bound and dissolved redox species. An advantage of this technique is that the SECM measurements are carried out under steady-state conditions, so that the complications caused by ohmic potential drop and charging current can be overcome. The contributions of direct electron tunneling through the monolayer and mediated ET to the overall interfacial charge transfer can be evaluated independently. The upper limits for the electron tunneling and bimolecular rate constants measurable by the developed technique are $\sim 10^8$ s^{-1} and $\sim 5 \times 10^{11}$ mol^{-1} cm^3 s^{-1}, respectively.

Acknowledgment. This work was supported by the Robert A. Welch Foundation, the National Science Foundation (CHE-0315558 and CHE-0109587), and PSC-CUNY.

JA038611P

(35) Marcus, R. A. *J. Chem. Phys.* **1965**, *43*, 679.
(36) Hurwitz, P.; Kustin, K. *Trans. Faraday Soc.* **1966**, *62*, 427.
(37) McManis, G. E.; Nielson, R. M.; Gochev, A.; Weaver, M. L. *J. Am. Chem. Soc.* **1989**, *111*, 5533.
(38) Marcus, R. A.; Sutin, N. *Biochim. Biophys. Acta* **1985**, *811*, 265.